Journal of Geophysical Research: Oceans

RESEARCH ARTICLE
10.1002/2017JC013583

Special Section:
The U.S IOOS Coastal and Ocean Modeling Testbed 2013–2017

Climate Change Projected to Exacerbate Impacts of Coastal Eutrophication in the Northern Gulf of Mexico

Arnaud Laurent[1], Katja Fennel[1], Dong S. Ko[2], and John Lehrter[3]

[1]Department of Oceanography, Dalhousie University, Halifax, NS, Canada, [2]Oceanography Division, Naval Research Laboratory, Stennis Space Center, Hancock County, MS, USA, [3]Department of Marine Sciences, University of South Alabama, Dauphin Island Sea Laboratory, Dauphin Island, AL, USA

Key Points:
- Hypoxia in the future is simulated to expand and become more severe due to lower O_2 solubility and enhanced density stratification
- Rising atmospheric pCO_2 results in a large drop in pH which will be further amplified by eutrophication
- The projected response to future conditions is larger in years with high freshwater discharge and upwelling-favorable wind

Supporting Information:
- Supporting Information S1
- Figure S1
- Figure S2
- Figure S3
- Data Set S1
- Data Set S2
- Data Set S3
- Data Set S4
- Data Set S5
- Data Set S6
- Data Set S7
- Data Set S8
- Data Set S9
- Data Set S10

Correspondence to:
A. Laurent,
arnaud.laurent@dal.ca

Citation:
Laurent, A., Fennel, K., Ko, D. S., & Lehrter, J. (2018). Climate change projected to exacerbate impacts of coastal eutrophication in the northern Gulf of Mexico. *Journal of Geophysical Research: Oceans*, *123*, 3408–3426. https://doi.org/10.1002/2017JC013583

Received 27 OCT 2017
Accepted 19 MAR 2018
Accepted article online 26 MAR 2018
Published online 15 MAY 2018

Abstract The continental shelf in the northern Gulf of Mexico experiences expansive seasonal hypoxic conditions and eutrophication-driven acidification in bottom waters. Rising surface ocean temperatures, freshwater and nutrient inputs, and atmospheric CO_2 will further exacerbate these conditions. Using a high-resolution, regional circulation-biogeochemical model, we simulated the spatiotemporal dynamics of oxygen and inorganic carbon in the northern Gulf of Mexico under present and a projected future (2100) climate state. Results indicate a modest expansion of the hypoxic zone, but more severe hypoxia and greater exposure to prolonged hypoxic conditions. The main drivers underlying these changes are a reduction in oxygen solubility (accounting for 60–74% of the change) and increased stratification (accounting for less than 40%). pH is projected to decrease across the shelf with lowest values in hypoxic waters where aragonite saturation will approach the saturation limit. In the model simulations, acidification is primarily driven by atmospheric and offshore CO_2 levels, while the enhancement in stratification only accounts for 7% or less of the total change in pH. Decreased buffering capacity and increased stratification in the future will enhance respiration-induced acidification (i.e., a decrease in bottom water pH by respired CO_2), which will amplify the climate-induced acidification. According to the model, the magnitude of future changes varies significantly from year to year. The largest effects are simulated in years with large freshwater discharge and upwelling-favorable winds.

Plain Language Summary The continental shelf in the northern Gulf of Mexico experiences eutrophication-driven seasonal low-oxygen conditions (hypoxia) and acidification (a decrease in bottom water pH by respired CO_2). Rising surface ocean temperatures, freshwater and nutrient inputs, and atmospheric CO_2 will further exacerbate these conditions. We simulated the variations of oxygen and inorganic carbon in the northern Gulf of Mexico at present and under a projected future (2100) climate state. Results indicate more severe and prolonged periods of hypoxia in the future due to reduced oxygen solubility in warmer waters and increased stratification. pH is projected to decrease significantly with lowest values in low-oxygen waters. Future acidification is primarily driven by rising atmospheric and offshore CO_2 levels. A decreased buffering capacity of seawater and increased stratification will enhance respiration-induced acidification, which will further amplify the climate-induced acidification. The magnitude of projected changes varies significantly from year to year, with the largest effects in years with large freshwater discharge and upwelling-favorable winds.

1. Introduction

Global warming and rising atmospheric carbon dioxide (CO_2) levels are projected to have profound effects on the upper ocean by the end of the century. Ongoing surface ocean warming (Cheng et al., 2017) is expected to intensify density stratification and may lead to a global deoxygenation (Keeling et al., 2010). Concurrently, the uptake of anthropogenic CO_2 is expected to decrease ocean pH and carbonate saturation levels (Feely et al., 2009; Sarmiento et al., 1998). This combination of stressors may have severe impacts on ocean ecosystems and fisheries (Bopp et al., 2013; Breitburg et al., 2015; Flynn et al., 2015), especially in coastal regions where eutrophication already leads to hypoxic and acidified conditions (Altieri & Gedan, 2014; Levin et al., 2015; Melzner et al., 2013).

Many coastal regions receive excessive nutrient inputs from rivers that stimulate algal growth and subsequent decomposition in bottom waters. The resulting oxygen consumption and dissolved inorganic carbon (DIC) production, in combination with stratified conditions, often result in hypoxic ($[O_2] < 62.5$ mmol O_2 m^{-3}), as well as acidified conditions (Cai et al., 2011; Rabouille et al., 2008). The occurrence of eutrophication-driven hypoxic conditions is a widespread and expanding phenomenon (Diaz & Rosenberg, 2008; Rabalais et al., 2010) and will likely be exacerbated by warming.

One of the world's largest coastal hypoxic zones is located in the northern Gulf of Mexico in the outflow region of the Mississippi and Atchafalaya Rivers (Rabalais et al., 2007). Seasonal hypoxia develops in the bottom boundary layer (BBL) every summer covering, on average, 14,000 km^2 (1985–2017, LUMCON, http://ww.gulfhypoxia.net). The hypoxic zone is also prone to respiration-induced acidification (Cai et al., 2011) shown to be controlled by benthic and lower water-column respiration rates (Laurent et al., 2017), although at present, acidified waters are still saturated with respect to aragonite and calcite (Cai et al., 2011; Laurent et al., 2017).

The timing, location, and magnitude of hypoxic conditions are variable in the northern Gulf and particularly sensitive to wind, freshwater discharge, and nutrient loads (Feng et al., 2012; Forrest et al., 2011; Mattern et al., 2013; Yu et al., 2015a). It has been shown that upwelling conditions promote the development of a large hypoxic area (Feng et al., 2014), especially when coinciding with elevated freshwater discharge, and affect the distribution of surface DIC and air-sea CO_2 exchange (Huang et al., 2015a).

In the future, warming may further exacerbate hypoxia in the northern Gulf of Mexico due to reduced oxygen solubility and increased density stratification (Justić et al., 1996; Lehrter et al., 2017), while rising atmospheric CO_2 is expected to lower bottom water pH (Cai et al., 2011). Uncertainties remain regarding the details, magnitude, relative importance, and variability of processes controlling future oxygen loss and acidification.

The objectives of this study are to investigate how oxygen and inorganic carbon dynamics are affected by a projected future climate state and to analyze the underlying mechanisms. Using a high-resolution, regional circulation-biogeochemical model, we compare present and projected future physical and biogeochemical properties on the shelf, quantify the relative importance of different mechanisms underlying the simulated changes in oxygen and DIC, and evaluate the importance of interannual variability on the simulated changes.

2. Methods

The coupled physical-biogeochemical model is an implementation of the Regional Ocean Modeling System (ROMS; Haidvogel et al., 2008) configured for the northern Gulf of Mexico shelf. The model has 20 terrain-following vertical layers and a horizontal resolution ranging from ~20 km in the southwestern corner to 1 km near the Mississippi River delta. Atmospheric forcing is prescribed with 3 h winds from the NCEP North American Regional Reanalysis data set (Mesinger et al., 2006) and with surface heat and freshwater flux climatologies (da Silva et al., 1994a, 1994b). Daily freshwater fluxes from the Mississippi and Atchafalaya Rivers are prescribed using freshwater transports estimated by the US Army Corps of Engineers at Tarbert Landing and Simmesport, respectively. Further details on setup and validation of the physical model are given in Hetland and DiMarco (2008, 2012), Marta-Almeida et al. (2013), and Fennel et al. (2016).

The biogeochemical model is based on the pelagic N-cycle model of Fennel et al. (2006, 2011) with the addition of carbonate chemistry (Fennel et al., 2008; Laurent et al., 2017), phosphate (Laurent et al., 2012; Laurent & Fennel, 2014, 2017), oxygen (Fennel et al., 2013), and river-derived dissolved organic matter (Yu et al., 2015b). A schematic of the model is presented in supporting information Figure S1. In total, the biogeochemical model includes 15 state variables: phytoplankton, chlorophyll, zooplankton, nitrate, ammonium, phosphate, oxygen, DIC, total alkalinity, and three detrital organic matter pools (small and large detritus, and river-derived DOM, all split into nitrogen and carbon pools). A detailed description of the biogeochemical model including parameter values is given in Laurent et al. (2017, see supporting information).

Initial and boundary conditions for nitrate, phosphate, and oxygen are prescribed from the NODC World Ocean Atlas. Other variables (except for DIC and TA) are set to small positive values. River nutrient and organic matter loads are based on monthly nutrient flux estimates from the U.S. Geological Survey (Aulenbach et al., 2007). River, initial and boundary conditions for DIC, and alkalinity are prescribed using shelf survey observations carried out between 2004 and 2010 (Cai et al., 2011; Huang et al., 2015b). Surface gas exchange is parameterized following Wanninkhof (2014).

Table 1
Model Forcing in the Present and Future Simulations

		Initial/boundary conditions				River		
	Wind	Physics	Biology	T^{air}	pCO_2^{air} (μatm)	Discharge	DIC	Nutrients
Present	NARR	IASNFS	WOA	Clim.	Clim.	USACE	Observed	USGS
Future	–	IASNFS (future)	+bias	+3°C	935.85	+10%	Adjusted to new pCO_2^{air}	−10%

Note. See text for details. The dash means no change between present and future simulations.

Sediment O_2 consumption (SOC) in the present simulation was parameterized as a function of bottom water temperature derived from diagenetic model simulations with realistic forcing. The diagenetic model was run under present and future bottom water conditions and two temperature-dependent parameterizations were derived (Laurent et al., 2016, 2017), $SOC = 0.614 \times 2^{T/5.474}$ (T in °C) under present conditions and $SOC = 0.593 \times 2^{T/5.927}$ under future conditions. Effluxes of ammonium, DIC, and alkalinity from the sediment are proportional to SOC using ratios of $NH_4^+ : SOC = 0.036$ mol N (mol O_2)$^{-1}$ (Fennel et al., 2013), $DIC : SOC = 0.9475$ mol C (mol O_2)$^{-1}$ (Laurent et al., 2017) and $TA : SOC = 0.036$ mol (mol O_2)$^{-1}$ (because 1 mol of alkalinity is produced in the sediment for each mol of NH_4^+). This parameterization includes the effect of sediment denitrification on alkalinity fluxes (Laurent et al., 2017). For the efflux of phosphate from the sediment, we assumed Redfield stoichiometry, i.e., $PO_4 : SOC = DIC : SOC/106$ mol P (mol O_2)$^{-1}$.

Two 6 year simulations, representing present and projected future conditions, were carried out. The simulations differ only in their initial and open boundary conditions, river discharge, and atmospheric temperature and pCO_2 but use identical wind forcing and river nutrient load (Table 1). The present simulation was run for the period 2005–2010 using physical initial and boundary conditions (i.e., water temperature, salinity, and currents) from the Intra-Americas Sea Nowcast-Forecast System (IASNFS; Ko et al., 2003; Ko & Wang, 2014; Lehrter et al., 2017). In the future simulation, physical boundary conditions are from a projection of the IASNFS model, which was run with 10% larger freshwater discharge and 3°C warmer air temperature (Lehrter et al., 2017). In our future simulation, river input and atmospheric forcing are based on the 2005–2010 daily record used in the present simulation. The mean Mississippi River discharge was increased by 10% (Sperna Weiland et al., 2012), and mean air temperature was increased by 3°C. This increase in air temperature is projected by the "business as usual" RCP8.5 scenario (Riahi et al., 2011) of the Max-Planck-Institute Earth System Model (MPI-ESM; Giorgetta et al., 2013; Ilyina et al., 2013) between present (2006–2010) and future (2096–2100) (see supporting information Figure S2). The MPI-ESM RCP8.5 simulation was used to prescribe future atmospheric pCO_2 and biogeochemical boundary conditions in our simulation.

Atmospheric pCO_2 was increased to 935.85 μatm, the 2100 annual average in MPI-ESM RCP8.5, in the future simulation. Biogeochemical initial and lateral boundary conditions were determined by calculating the differences between future and present biogeochemical values at an offshore central northern Gulf location (27°N, 90°W) in MPI-ESM RCP8.5 (see supporting information Figure S3) and adding these to the present initial and boundary conditions. Surface nitrate, phosphate, and oxygen concentrations decrease in the future, whereas DIC and alkalinity increase. The change is small for nutrients, moderate for oxygen and significant for DIC and alkalinity.

We used the same river nutrient load for the present and future simulations. The imposed 10% increase in freshwater discharge in the future simulation implies that nutrient concentrations in river water were slightly diluted. The river DIC concentration was adjusted by calculating the deviation from equilibrium for present river DIC and then adding this deviation to the new equilibrium in the future simulation. Both the present and future simulations were spun up for 3 years.

3. Results

3.1. Changes in Physical and Biogeochemical Properties on the Shelf

The future surface and open Gulf forcing conditions had a significant effect on the northern Gulf of Mexico shelf waters (Figure 1). The physical properties of the shelf waters changed significantly between present and future (Figure 2 and Table 2). Surface and bottom water temperatures in summer increase by 2.69 and

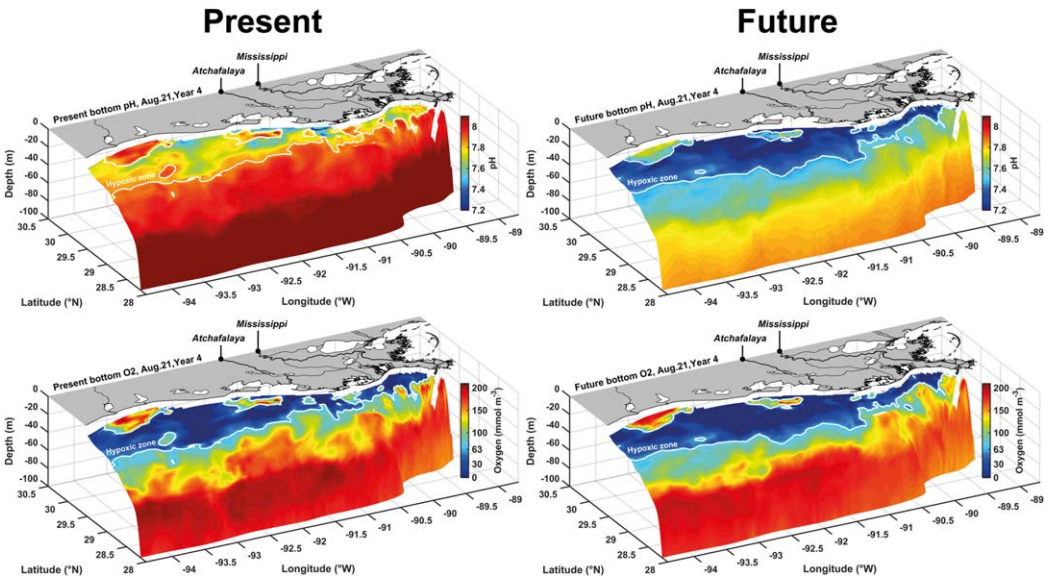

Figure 1. Present and future bottom (top row) pH and (bottom row) oxygen simulated on 21 August (year 4). The white contour line indicates the limit of the hypoxic zone.

2.23°C, respectively. Surface and bottom salinities in summer decrease by 0.48 and 0.02, respectively. Surface salinity is mainly controlled by freshwater discharge whereas bottom salinity is also influenced by offshore waters, which are saltier in the future simulation. Overall, the warmer and fresher waters have a lower density, decreasing at the surface on average by 1.28 kg m^{-3} and at the bottom by 0.76 kg m^{-3}. Since the change in density is larger at the surface, the potential energy anomaly (PEA; J m^{-3}), a measure of stratification, increases in summer by +12.35 J m^{-3} on average (Table 2). The intensification of stratification is also indicated by the vertical profiles of the squared Brunt-Väisälä frequency (N^2), another measure of water-column stratification (Figure 2).Warmer water temperature in the future simulation results in lower oxygen saturation concentrations ($\Delta O_2^{sat} = -9.8$ mmol m^{-3} in winter, Table 2) and thus lower oxygen concentrations in surface waters ($\Delta O_2 = -9.1$ mmol m^{-3} in winter). Future saturation concentrations are lower throughout the year, contributing to the mean loss of oxygen in the future simulation (Table 3 and Figure 3). In summer, the future surface oxygen concentration is 3.4% lower on average than at present ($\Delta O_2 = -7.3$ mmol m^{-3}). This difference is very similar to the decrease in oxygen saturation (changes in oxygen saturation are somewhat larger than those for oxygen concentration; this discrepancy may be attributed to a modest increase in primary production, see section 3.2.1). Most of the surface oxygen variation is thus explained by the change in surface temperature. In bottom waters, the change in O_2 concentration is more pronounced with an average decrease of 9.4% ($\Delta O_2 = -12.3$ mmol m^{-3}). Assuming that bottom waters were last in contact with the atmosphere in winter, the change in surface oxygen (due to the lower saturation concentration) accounts for 74% of the decrease in bottom oxygen concentration. This calculation assumes that variations in bottom water oxygen due to lateral advection are negligible and that variations in O_2 are mainly driven by local processes. If we assume instead that bottom waters were last in contact with the atmosphere in summer (during a tropical storm for example), the change in surface O_2 would account for only 60% of the variation in bottom O_2 concentration. Thus, between 26 and 40% of the oxygen loss in bottom waters under future climate conditions is controlled by factors other than changing oxygen saturation.

The loss of oxygen results in an increase in the extent and duration of hypoxia in the future. Time-integrated hypoxic area increases by 26% and hypoxic volume by 39% on average, with significant year-to-year variations (Table 4). Bottom waters also tend to be hypoxic for longer (Table 4). Hypoxia occurs continuously for more than a week in more than 25.4 × 10^3 km^2 of the shelf in the future simulation, which is a 21% increase from the present (Table 4). For periods over 2 weeks and 1 month the area increases to 14.1 × 10^3 km^2 (+44%) and 2.8 × 10^3 km^2 (+75%), respectively. The increase in hypoxia duration results in more frequent low-oxygen and anoxic waters (Table 4). On average, the time-integrated area of low oxygen increases by 33% for $O_2 < 40$ mmol m^{-3}, by 42% for $O_2 < 20$ mmol m^{-3} and by 57% for anoxic waters.

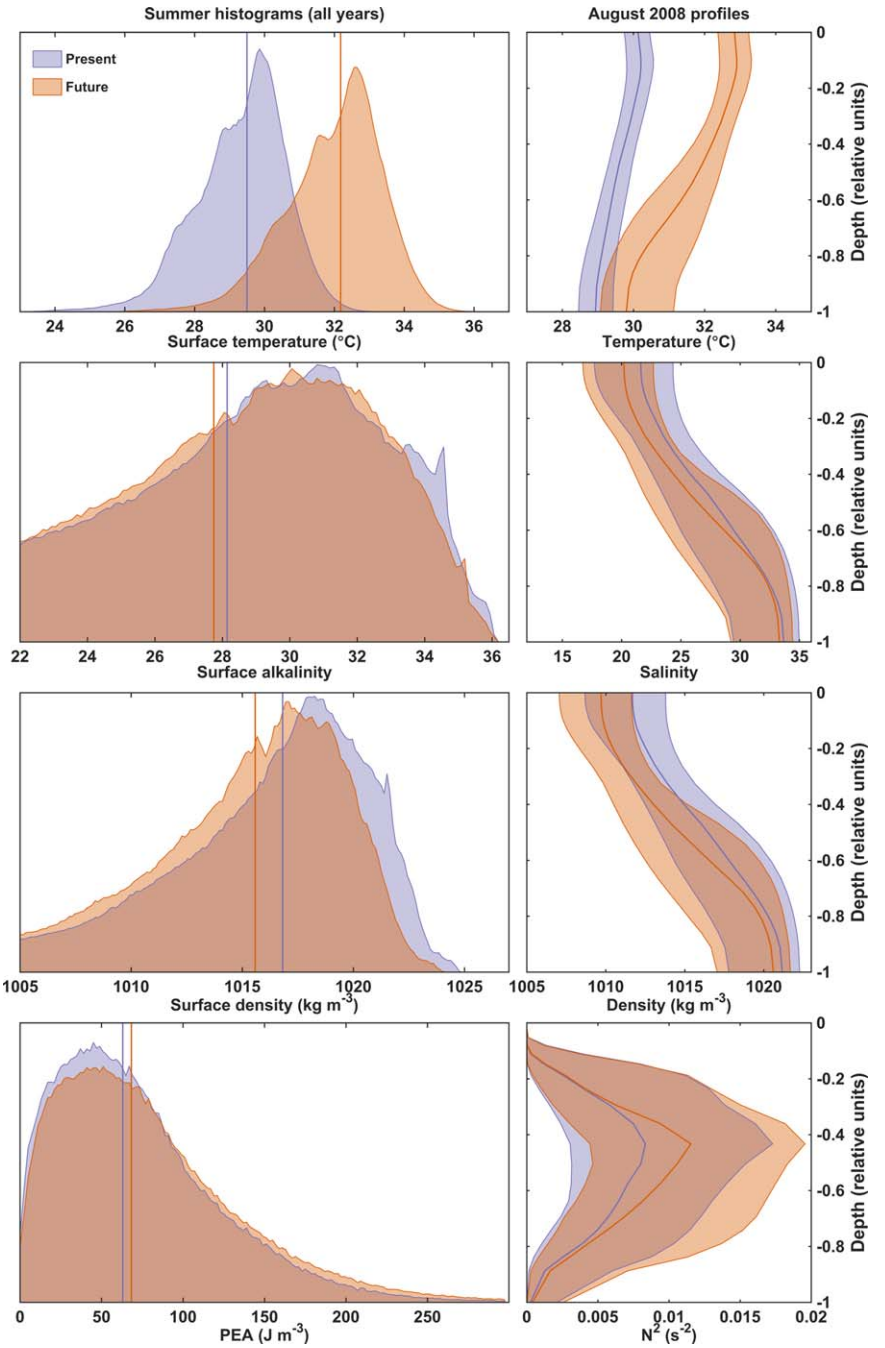

Figure 2. Present and projected future physical conditions on the shelf in summer. (left) Frequency distribution of surface water temperature, salinity and density, and potential energy anomaly (PEA) as measure of water-column stratification (June–September, all years). PEA data are restricted to the hypoxic zone. (right) Vertical profiles in August (year 4) of medians and 25th to 75th percentile ranges of temperature, salinity, density, and squared Brunt-Väisälä frequency (N^2) in the region where hypoxia typically occurs (0–20 m, 91.2°W–89.0°W).

Oxygen and inorganic carbon variables are strongly correlated in the present and future simulations (Figure 4). However, a major difference between oxygen and inorganic carbon variables is the drastic change in the mean of the latter (Figures 1 and 4 and Table 3). In the future, large increases in atmospheric pCO_2 and DIC of open ocean waters (reflected in our lateral boundary conditions) have a significant impact on the carbonate system. Summer surface pCO_2 increases to 982.4 μatm and DIC to 2311.7 mmol m^{-3} (Table 3). Alkalinity increases to 2,490.9 mmol m^{-3} because of an increase in boundary alkalinity predicted

Table 2
Average Physical Properties on the Shelf in the Simulation With Future Climate

Variable	Units	Period	Year 1	Year 2	Year 3	Year 4	Year 5	Year 6	All
Discharge	$\times 10^9$ m^3	May–July	130.4	120.9	179.2	315.1	287.5	240.4	212.2
		July	35.2	26.4	55.5	85.3	57.4	70.3	55.0
Alongshore wind stress	N m^{-3}	July	−0.020	−0.011	−0.002	−0.006	+0.007	−0.045	−0.013
		August	−0.014	−0.011	−0.024	+0.003	−0.007	−0.006	−0.001
Temperature	°C	Summer	32.72	32.61	32.41	32.35	32.52	32.02	32.4
			+2.86	*+2.68*	*+2.71*	*+2.68*	*+2.63*	*+2.57*	*+2.69*
Salinity		Summer	26.98	28.48	26.22	22.14	25.44	25.42	25.78
			−1.13	*−0.41*	*−0.66*	*−0.84*	*−0.26*	*+0.36*	*−0.49*
Density	kg m^{-3}	Summer	1,014.9	1,016.0	1,014.4	1,011.4	1,013.8	1,014.0	1,014.1
			−1.83	*−1.23*	*−1.41*	*−1.53*	*−1.09*	*−0.60*	*−1.28*
PEA	J m^{-3}	Summer	103.79	85.98	99.54	167.48	128.19	111.54	116.09
			+28.14	*+8.62*	*+9.71*	*+25.43*	*+2.81*	*−0.60*	*+12.35*
BBL	m	Summer	3.61	3.99	3.92	4.21	3.86	3.75	3.89
			−1.26	*−0.76*	*−1.21*	*−1.05*	*−0.38*	*−0.44*	*−0.85*
O_2 concentration at 100% saturation	mmol m^{-3}	Winter	232.68	229.45	230.88	229.38	231.08	234.22	231.28
			−9.47	*−10.34*	*−9.50*	*−9.75*	*−10.04*	*−9.51*	*−9.77*
		Summer	190.62	189.36	192.39	196.89	193.00	194.45	192.78
			−7.68	*−7.80*	*−7.80*	*−7.74*	*−8.01*	*−8.62*	*−7.94*

Note. Temperature, salinity, density, and O_2 concentration at 100% saturation are at the surface. Numbers in italic represent the difference between present and future simulations. Positive alongshore wind stress is upwelling-favorable and negative alongshore wind stress is downwelling favorable. Alongshore wind stress is calculated from the u-wind speed component at a midshelf location (28.64°N, −90.60°W). BBL refers to bottom boundary layer thickness.

by MPI-ESM RCP8.5. The result of these changes is a decrease in surface water pH by 0.3–7.8 on average in summer under future climate conditions. The changes occur throughout the water column (Figure 3) but are more pronounced in bottom waters where DIC increases to 2,414.0 mmol m^{-3} ($\Delta_{DIC} = +232.0$), alkalinity to 2,523.9 mmol m^{-3} ($\Delta_{TA} = +75.2$) and pH decreases to 7.58 ($\Delta_{pH} = -0.37$) on average in summer (Table 3 and Figure 3). In hypoxic waters, average pH is 7.39 ($\Delta_{pH} = -0.34$). Note that the standard deviation for summer pCO_2 on the shelf (all years) is 407.6 μatm at the surface and 1,111.4 μatm at the bottom, indicating large spatial and temporal variability. pCO_2 reached very high values in some areas of the shelf, mostly in bottom hypoxic waters ($pCO_2 > 4{,}000$ μatm). The carbonate saturation state near the bottom drops significantly but remains well above the saturation limit for aragonite $\Omega_{Ar} = 1.82$ (–44%) and calcite $\Omega_{Ca} = 2.73$ (–45%) for most of the shelf in summer. However, the aragonite saturation state reaches values close to or below the saturation limit in hypoxic waters ($\Omega_{Ar} = 1.05 \pm 0.29$ SD) and the time-integrated area of undersaturated waters increases from 8.7 km^2 yr on average in the present to 116.6 km^2 yr in the future simulation.

3.2. Interannual Variability in Physical Conditions

The changes between present and future vary in magnitude from year to year. Differences in the alongshore wind direction (upwelling versus downwelling favorable), and magnitude and phenology of river discharge influence the spatiotemporal distribution of stratification and thus the response to future forcing. For example, in year 4 (2008), the freshwater discharge was unusually large in July (Table 2), wind forcing was weak from mid-June to mid-July and upwelling-favorable wind occurred in August (henceforth referred to as the "wet/upwelling" year). A large amount of freshwater was therefore present on the shelf during the hypoxic season. Future average PEA in summer is larger by 25.0 J m^{-3} compared to the present under that year's river and wind forcing. Conversely, in year 2 (2006), discharge was small and wind was downwelling favorable (henceforth referred to as the "dry/downwelling" year). In this case, future salinity was highest and PEA lowest increasing only by +8.5 J m^{-3} on average between present and future (Table 2). A comparison of midsummer surface salinity for the "wet/upwelling" and "dry/downwelling" years (Figure 5) shows the large extent of plume waters in the wet/upwelling year, covering most of the shelf, in contrast to a much smaller extent of freshwater in the dry/downwelling year, when the plume was confined to the Mississippi delta and Atchafalaya Bay regions. Finally, year 6 (2010), referred to hereafter as the "strong wind" year, had moderate discharge with a series of strong downwelling-favorable wind events in late June to July and from late August through September (Table

Table 3
Average Biogeochemical Properties on the Shelf in the Simulation With Future Climate

Variable	Year 1	Year 2	Year 3	Year 4	Year 5	Year 6	All
Surface waters (summer)							
O_2 (mmol m^{-3})	208.5	205.4	211.7	218.0	207.4	213.3	210.7
	−7.15	*−8.46*	*−7.80*	*−6.63*	*−7.43*	*−6.66*	*−7.35*
pH	7.79	7.78	7.81	7.82	7.79	7.82	7.80
	−0.29	*−0.31*	*−0.30*	*−0.28*	*−0.30*	*−0.29*	*−0.30*
TIC (mmol m^{-3})	2,312.3	2,321.1	2,319.9	2,299.9	2,300.0	2,318.9	2,312.0
	+190.3	*+210.5*	*+198.3*	*+161.8*	*+197.2*	*+186.3*	*+190.7*
TA (mmol m^{-3})	2,495.9	2,511.9	2,506.7	2,463.2	2,472.9	2,501.7	2,492.0
	+50.7	*+63.4*	*+56.5*	*+35.8*	*+62.6*	*+58.2*	*+54.5*
pCO_2 (μatm)	983.8	972.1	960.5	988.1	1,005.2	941.7	975.2
	+557.6	*+568.2*	*+553.0*	*+542.1*	*+577.7*	*+528.8*	*+554.6*
Ω_{Ar}	2.68	2.72	2.73	2.55	2.58	2.69	2.66
	−1.44	*−1.54*	*−1.50*	*−1.36*	*−1.43*	*−1.40*	*−1.45*
Ω_{Ca}	4.07	4.11	4.17	3.98	3.95	4.12	4.07
	−2.23	*−2.37*	*−2.33*	*−2.14*	*−2.23*	*−2.21*	*−2.25*
Bottom waters (summer)							
O_2 (mmol m^{-3})	112.2	118.5	117.6	114.8	109.1	135.8	118.0
	−18.85	*−9.80*	*−16.05*	*−16.59*	*−7.26*	*−5.45*	*−12.33*
pH	7.55	7.57	7.59	7.57	7.55	7.64	7.58
	−0.38	*−0.37*	*−0.37*	*−0.38*	*−0.36*	*−0.34*	*−0.37*
TIC (mmol m^{-3})	2,422.8	2,414.4	2,413.4	2,417.3	2,422.4	2,395.4	2,414.3
	+237.0	*+234.7*	*+236.8*	*+232.8*	*+232.0*	*+221.4*	*+232.4*
TA (mmol m^{-3})	2,522.3	2,528.9	2,529.4	2,515.6	2,522.3	2,528.1	2,524.5
	+69.7	*+77.4*	*+75.0*	*+70.7*	*+82.0*	*+77.3*	*+75.4*
pCO_2 (μatm)	1,942.7	1,756.5	1,677.3	1,717.7	1,837.6	1,391.7	1,720.6
	+1,274.9	*+1,141.4*	*+1,095.8*	*+1,124.7*	*+1,172.4*	*+847.9*	*+1,109.5*
Ω_{Ar}	1.76	1.87	1.87	1.69	1.72	2.01	1.82
	−1.52	*−1.45*	*−1.50*	*−1.49*	*−1.34*	*−1.39*	*−1.45*
Ω_{Ca}	2.64	2.79	2.81	2.56	2.58	3.02	2.73
	−2.30	*−2.20*	*−2.29*	*−2.28*	*−2.05*	*−2.13*	*−2.21*

Note. Numbers in italic represent the difference between present and future simulations.

2) interrupted by a period of upwelling-favorable wind in August. In the strong wind year, surface salinity increased 0.36 and PEA did not change significantly ($\Delta_{PEA} = -0.62$ J m^{-3}) between present and future simulations. This interannual variability needs to be taken into account to understand the effects of physical drivers on future changes in biogeochemistry.

3.3. Mechanisms Underlying the Biogeochemical Changes

3.3.1. Oxygen

Several processes that affect oxygen sources and sinks are involved in generating the future decrease in oxygen concentration. Above, we quantified the saturation-dependent effect on bottom oxygen, which accounts for 60–74% of the decrease. The remaining 26–40% result from changes in biological rates, stratification, and/or the thickness of the bottom boundary layer where hypoxia occurs.

In the future simulation, vertically integrated primary production in summer is 73.5 mmol O_2 m^{-2} d^{-1} on average, which represents a modest 2.4% increase from the present run. The total oxygen sink in sediment and water column over the same period is 78.5 mmol O_2 m^{-2} d^{-1} on average and did not change significantly (+0.2%). Water-column respiration (53.0 mmol O_2 m^{-2} d^{-1}) increased by 0.9 mmol O_2 m^{-2} d^{-1} (+1.6%), nitrification (4.9 mmol O_2 m^{-2} d^{-1}) did not change, and SOC (20.6 mmol O_2 m^{-2} d^{-1}) decreased by 0.7 mmol O_2 m^{-2} d^{-1} (–3.2%). This latter decrease is explained by a faster remineralization of organic matter in the sediment at warmer temperature, which resulted in somewhat higher SOC in spring and lower SOC in summer. The annual average of SOC did not change. Overall, the average change in oxygen concentration in the water column resulting from biological sources and sinks is +1.6 mmol O_2 m^{-2} d^{-1}. Biological processes were therefore a small net source of oxygen in the future simulation.

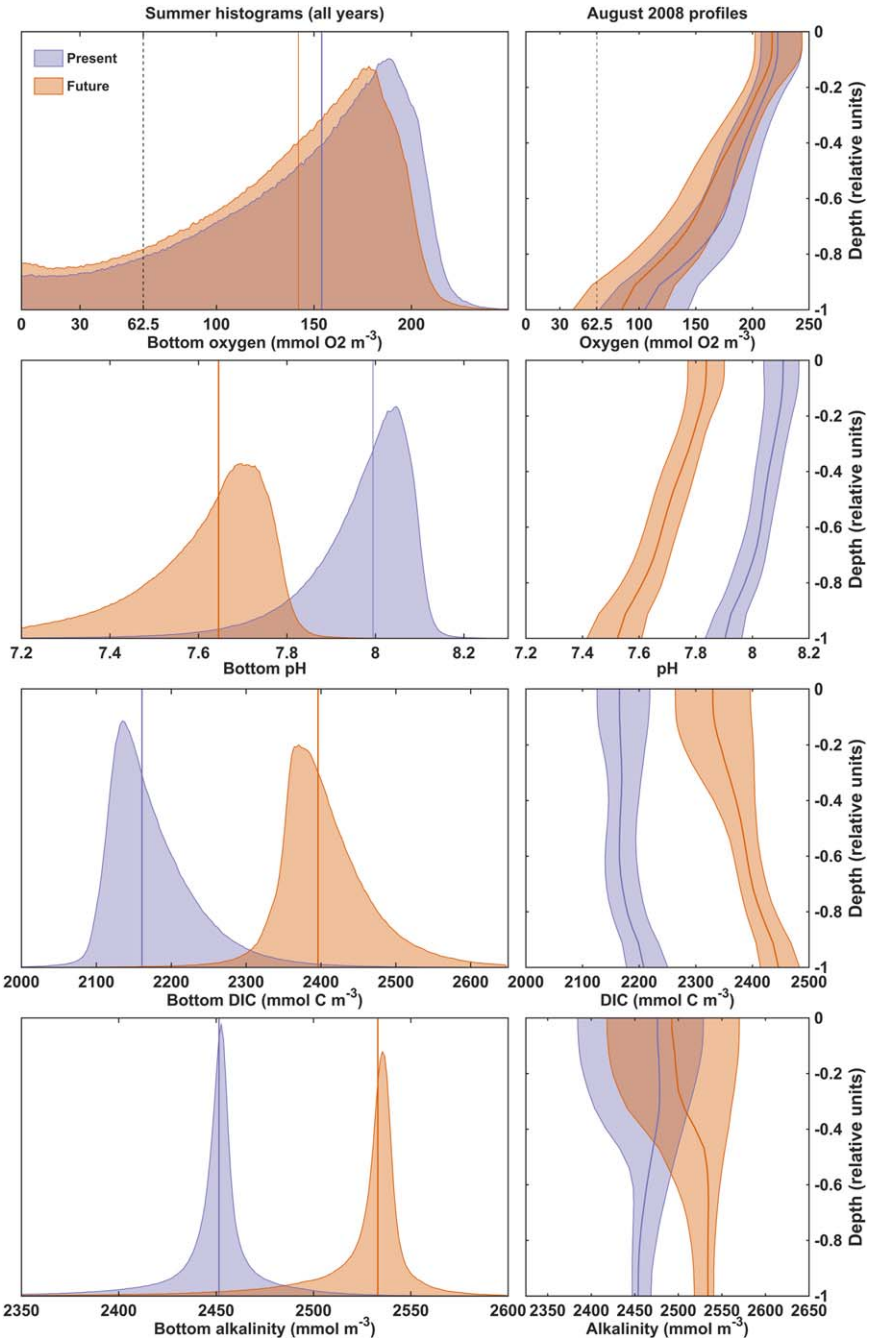

Figure 3. Biogeochemical conditions on the shelf in summer. (left) Frequency distribution oxygen, pH, DIC, and alkalinity in bottom waters (June–September, all years). (right) Vertical profiles of medians and 25th to 75th percentile ranges of oxygen, pH, DIC, and alkalinity in the regions where hypoxia typically occurs (0–20 m, 91.2°W–89.0°W) for August 2008.

The increase in stratification strength and thinning of the bottom boundary layer in the future simulation contribute to the amplification of oxygen drawdown in bottom waters. The change in stratification is not uniform over the 6 years simulated. Therefore, to assess the impact of stratification on the oxygen decrease between present and future, we discuss the 3 different years introduced in section 3.2: the wet/upwelling year where hypoxia increased significantly, the dry/downwelling year with moderate increase in hypoxia, and the strong wind year where hypoxia changed only slightly.

During the wet/upwelling year (year 4), hypoxia increased over most of the shelf in the future (Table 4 and Figures 6a and 7), in particular in the midshelf region (Figures 1 and 6a). Upwelling moves cold slope water

Table 4
Metrics of Hypoxic Extent and Exposition to Hypoxia/Anoxia

Variable	Year 1	Year 2	Year 3	Year 4	Year 5	Year 6	All	SD
Time-integrated hypoxic area (HA) and hypoxic volume (HV)								
HA ($\times 10^3$ km^2 yr)	1,266	1,004	913	1,138	1,123	583	1,004	239
	+280	*+117*	*+332*	*+356*	*+97*	*+65*	*+208*	*+29*
HV ($\times 10^9$ m^3 yr)	3,398	2,471	2,320	2,904	2,734	1,191	2,503	744
	+986	*+417*	*+1,165*	*+1,187*	*+336*	*+96*	*+698*	*+159*
Time-integrated area with low O_2 ($\times 10^3$ km^2 yr)								
$O_2 < 40$	966	701	648	747	773	297	688.7	220.3
	+244	*+111*	*+287*	*+265*	*+90*	*+18*	*+169.4*	*+43.0*
$O_2 < 20$	752	470	446	474	525	140	467.8	196.0
	+226	*+107*	*+219*	*+189*	*+83*	*+0*	*+137.3*	*+54.0*
Anoxic	524	246	226	227	278	45	257.8	154.0
	+185	*+91*	*+117*	+108	*+69*	*−6*	*+94.0*	*+53.5*
Area exposed to continuous hypoxia ($\times 10^3$ km^2)								
> 1 week	35.2	23.9	29.5	25.5	24.3	14.1	25.4	7.0
	+4.7	*+1.1*	+12.9	+6.9	+0.8	−0.3	+4.4	+1.2
> 2 weeks	27.7	13.0	11.6	15.6	13.0	3.5	14.1	7.9
	+7.2	+3.7	*+8.7*	*+6.5*	*+0.7*	*−0.8*	*+4.3*	*+1.5*
> 1 month	6.3	2.6	1.3	3.2	3.3	0	2.8	2.1
	+2.3	*+1.6*	*+0.9*	*+2.2*	*+0.5*	*0*	*+1.2*	*+0.6*

Note. Numbers in italic represent the difference between present and future simulations. O_2 is in mmol m^{-3}.

onto the shelf resulting in stronger stratification. The future forcing of higher surface heat flux (T^{air} +3°C) and larger river discharge (+10%) further stratifies the water over most of the shelf. The change in stratification strength (measured as PEA) is negatively correlated with the change in bottom oxygen in summer during the wet/upwelling year ($r = -0.56$, $p < 0.01$, i.e., ΔO_2 is more negative with increasing ΔPEA), and positively correlated with the change in hypoxic area (ΔH; $r = 0.59$, $p < 0.01$, Figures 7 and 8). A time series at a midshelf station off Terrebonne Bay illustrates the relationship between ΔPEA and ΔO_2 during the hypoxic season of the wet/upwelling year (Figure 9). For that year, the bottom boundary layer thickness (ΔBBL) is 20% thinner in the future. ΔBBL is positively correlated with ΔO_2 from June to September ($r = 0.64$,

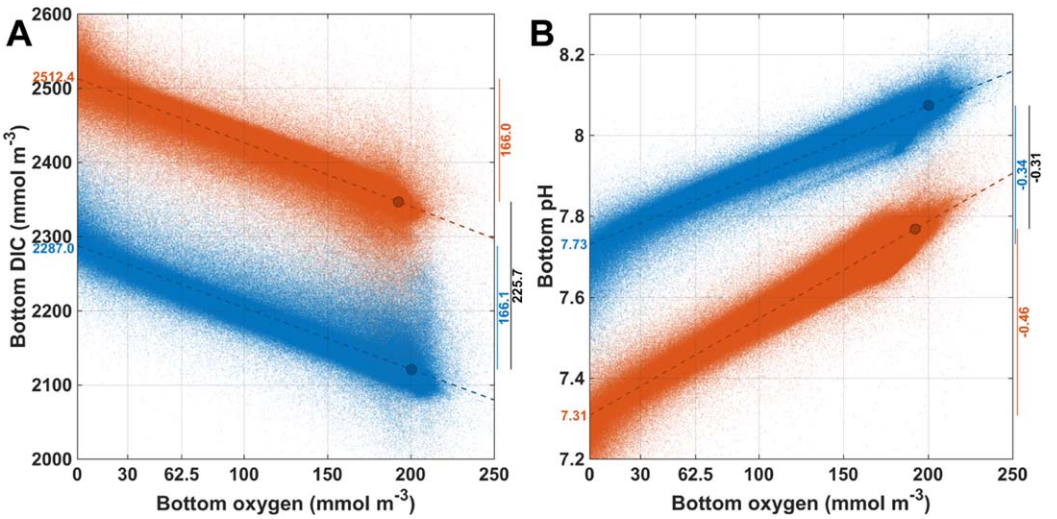

Figure 4. Relationships between (a) O_2 and DIC and (b) O_2 and pH in bottom waters in summer. Relationships are calculated for the present (blue) and future (orange) simulations. Dashed lines are the fit for each relationship. The scattered dots are the model data points. The dots on the dashed lines are the values for O_2-saturated surface waters in summer (see Table 2). Numbers on the left side of each figure indicate the values in anoxic conditions. Numbers on the right side of each figure indicate the future – present difference at surface O_2 saturation (black), the difference between O_2 saturation and anoxia for the present (blue) and future (orange) simulations.

$p < 0.01$) and negatively correlated with ΔH ($r = -0.51$, $p < 0.01$, Figure 8). The lack of change in ΔH with increasing ΔBBL indicates that these waters were above or close to the hypoxic level in the present simulation.

During the dry/downwelling year (year 2), hypoxia intensifies near the Mississippi and Atchafalaya River mouths and weakens elsewhere (Figure 6b). Downwelling combined with less rainfall reduces the stratification on the shelf in general (Figure 7). In this year, the future hypoxic area increases only in August (Figure 7), likely mainly due to a larger increase in heat flux and river flow. This is also the year with the smallest increase in future stratification of the 6 years simulated (Table 2). The water column remains weakly stratified over most of the shelf and there is no relationship between ΔPEA and ΔO_2 ($r = 0.06$, $p = 0.49$).

During the year with strong wind (year 6), stratification and hypoxia are controlled by a series of wind events that include passages of hurricanes and tropical storms. The wind events produce strong mixing and increase the contact between bottom water and the atmosphere, and changes between present and future are small (Figure 7). The overall size and duration of the hypoxic area does not change significantly in this year, but some relocation occurs over the shelf (Figure 6c). A weak correlation exists between ΔPEA and ΔO_2 ($r = -0.25$, $p < 0.01$), but the magnitude of the changes is very small.

3.3.2. Carbon

Oxygen sources and sinks are also sinks and sources of DIC, hence, the processes affecting oxygen also affect DIC and pH. As discussed above, changes in primary production and respiration have a negligible

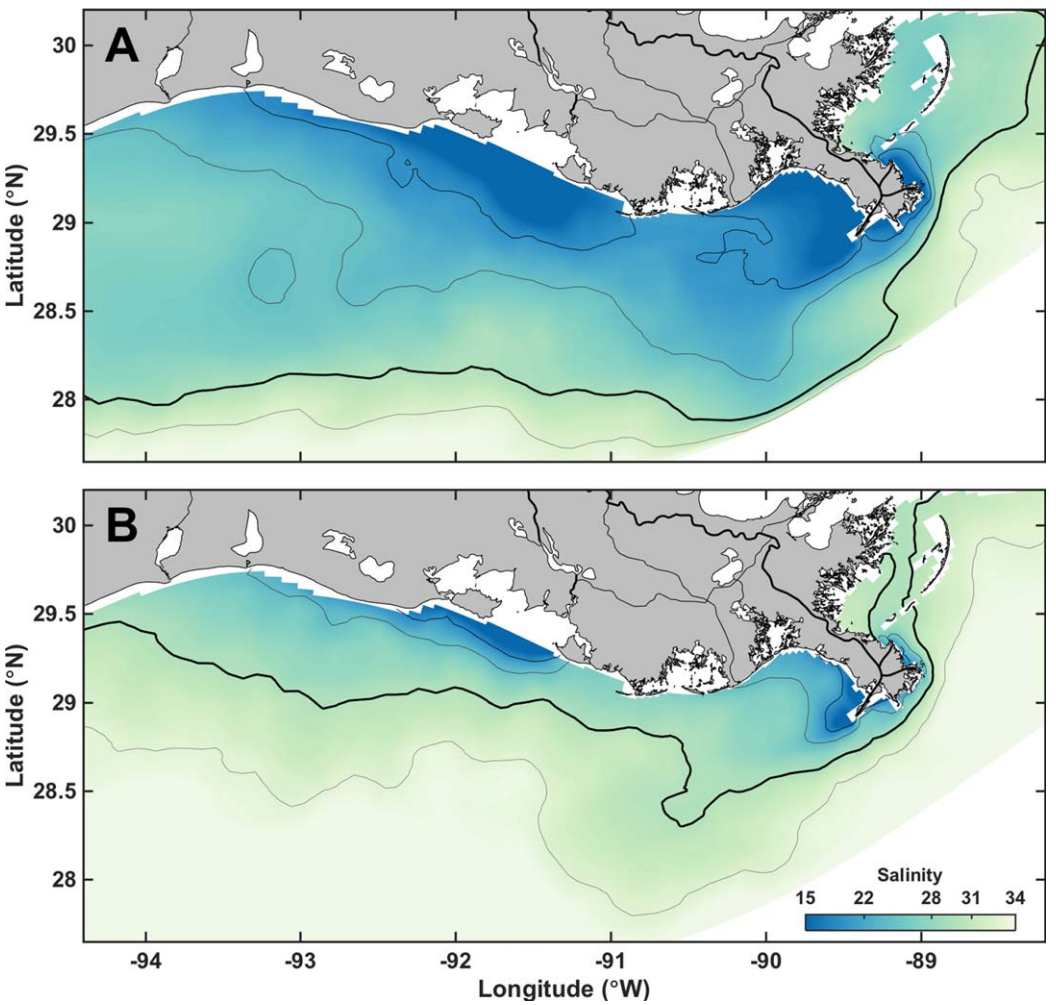

Figure 5. Average future surface salinity in July–August during (a) the wet/upwelling year (year 4) and (b) the dry/downwelling year (year 2). The isolines indicate salinities of 33, 30 (thick), 25, and 20.

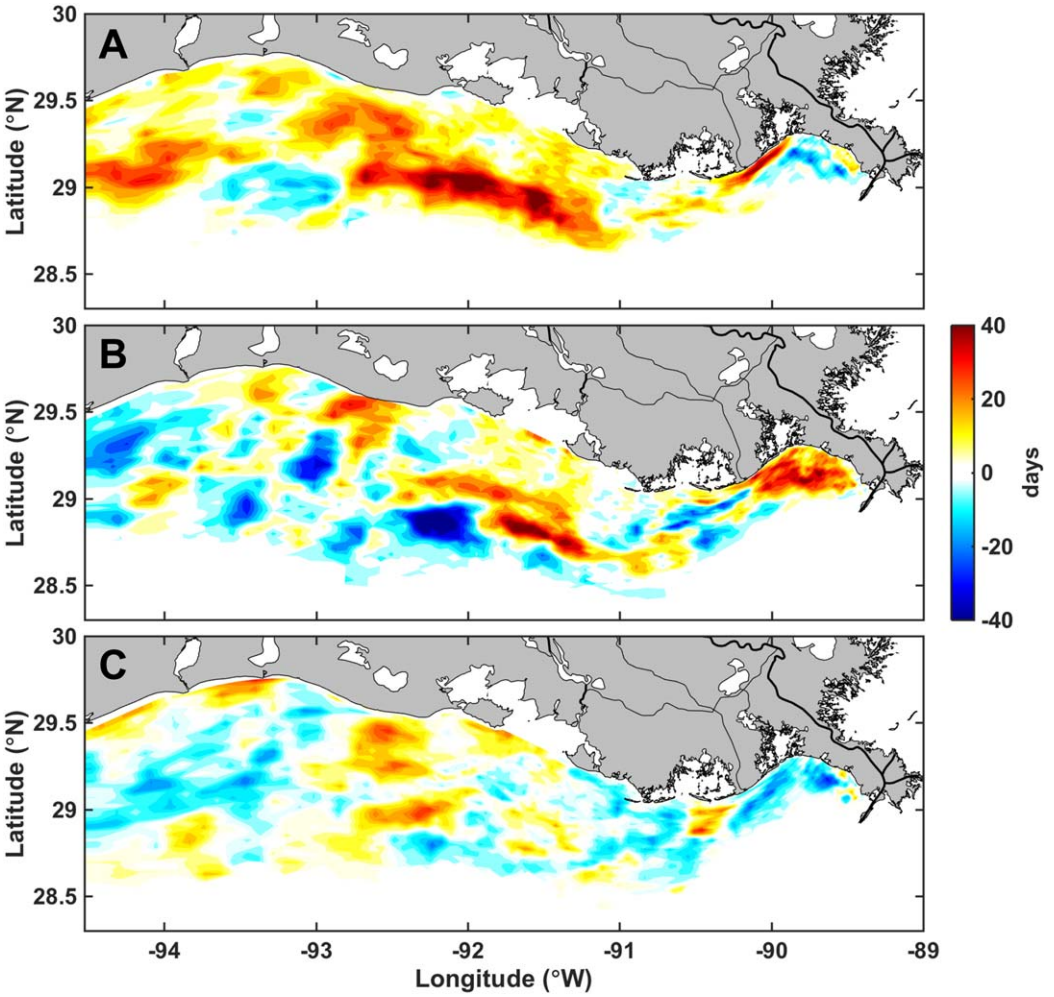

Figure 6. Change in the number of hypoxia days during the (a) upwelling year, (b) downwelling year, and (c) strong wind year. The change in hypoxia days is calculated as future – present.

effect on oxygen changes, and the same is true for the inorganic carbon variables, while the intensification of stratification that amplifies oxygen drawdown also intensified the eutrophication-induced acidification in the future simulation. The year-to-year variability in oxygen associated with interannual changes in river discharge and wind forcing (see section 3.3.1) apply also to pH (Figure 10). ΔpH is larger over most of the shelf in the wet/upwelling year (Figure 10a) and the spatial patterns are very similar to those found for hypoxia (Figures 1 and 6a). During this year, the change in bottom pH in summer is negatively correlated with the change in PEA ($r = -0.38$, $p < 0.01$, i.e., ΔpH is more negative with increasing ΔPEA), and positively correlated with the change in bottom boundary layer thickness ($r = 0.72$, $p < 0.01$). The time series at the coastal station illustrates this response to stratification during the wet/upwelling year (Figure 9). The spatial patterns in ΔpH are also similar to the changes in hypoxia during the dry/downwelling year (Figure 10b). As for hypoxia, the spatial changes in ΔpH are small during the strong wind year (Figure 10c).

However, the largest change in DIC and pH is driven by the increase in atmospheric pCO_2 (ΔpCO_2^{atm}). To assess the different contributions, we ran two additional simulations. A simulation with present biogeochemical initial and forcing conditions, but future physical forcing (T^{air} +3°C, discharge +10%, future boundary physics), and a simulation with future biogeochemical initial and forcing (future pCO_2^{atm} and biogeochemical boundary conditions), but present physical forcing. The results from the additional simulations indicate that in surface waters, future physical forcing (mainly atmospheric temperature) results in a ΔpH of

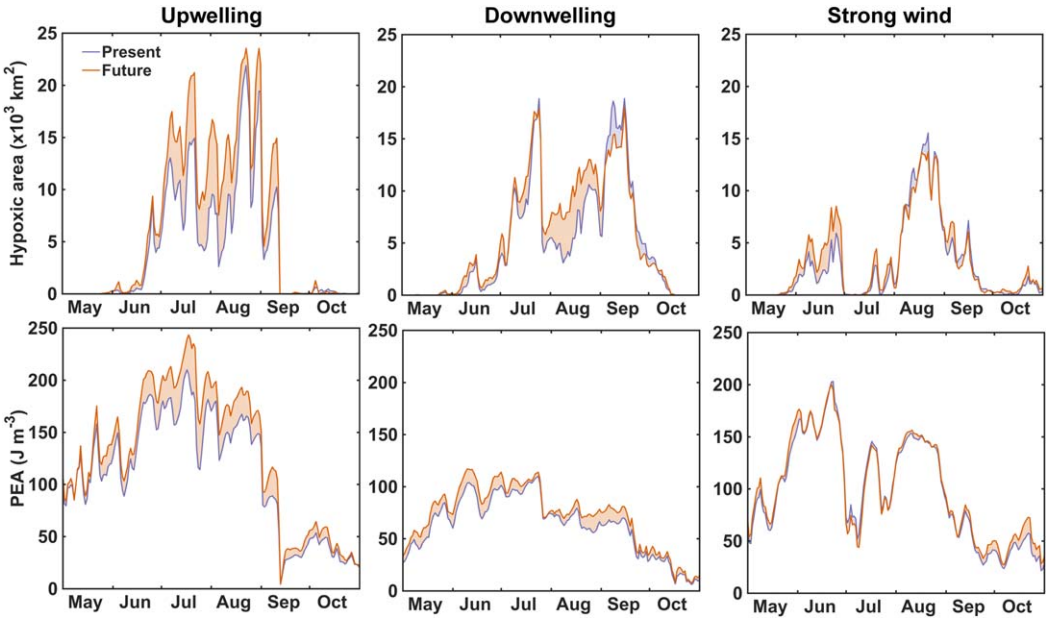

Figure 7. Time series of hypoxic area and average PEA on the shelf in the present (blue) and future (orange) simulations for (left) the upwelling year (year 4), (middle) the downwelling year (year 2), and (right) the strong wind year (year 6). The orange and blue shaded areas indicate, respectively, an increase or decrease between present and future.

−0.02, while future biogeochemical forcing results in a ΔpH of −0.29. In bottom waters, future physical forcing (i.e., changes in temperature, stratification and bottom boundary layer thickness) results in a ΔpH of −0.03 and future biogeochemical forcing results in a ΔpH of −0.33. Thus, the change in physics contributes about 9% to the total change in pH (5% for temperature and 4% for stratification/bottom boundary layer thickness). The remaining 91% of ΔpH is associated with biogeochemical boundary conditions.

Another method for quantifying the processes contributing to changes in the carbonate system is to assess the changes in the relationship between O_2, pH, and DIC in the present and future simulations (Figure 4). The total change in DIC (ΔDIC) and pH (ΔpH) at the surface can be quantified by calculating ΔDIC and ΔpH at surface O_2 saturation (Figure 4). In the future simulation, ΔDIC = +225.7 mmol m^{-3} and ΔpH = −0.31.

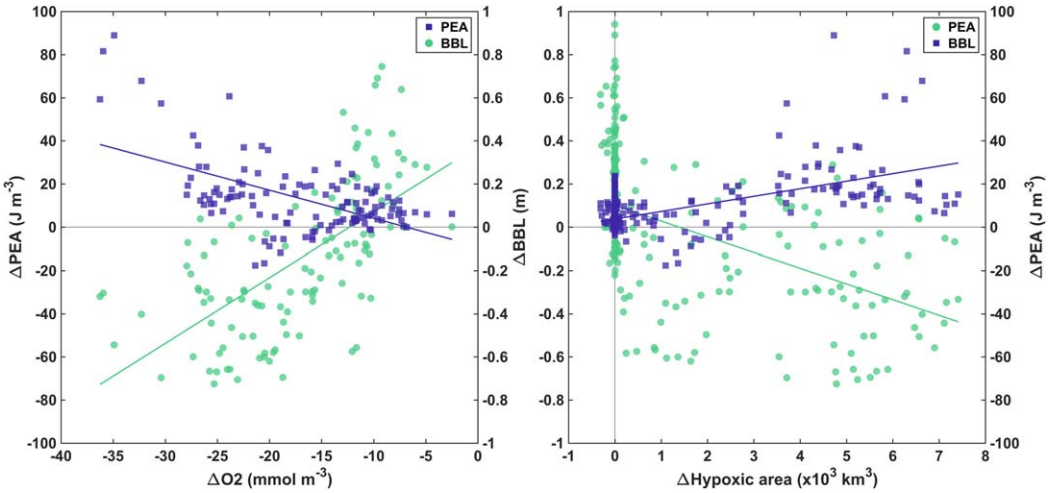

Figure 8. Daily, shelf-averaged change (left) in summer bottom water O_2 concentration (June–September) and (right) in the size of the hypoxic area during the wet/upwelling year (year 4) versus the change in PEA (blue squares) and BBL thickness (green dots). The change is calculated as future – present. The lines represent linear fits between *x* axis and *y* axis variable.

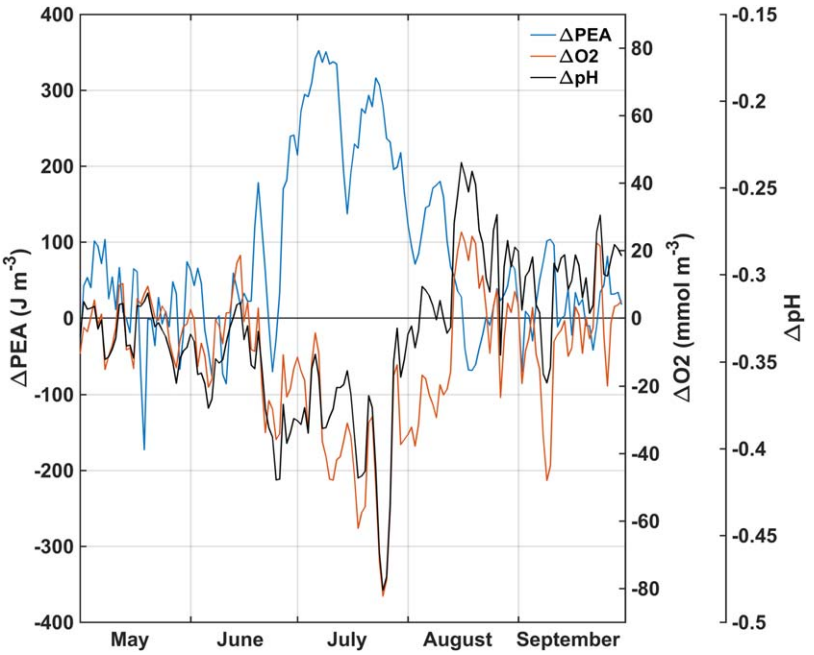

Figure 9. Time series of the change in PEA (ΔPEA, blue), bottom O_2 concentration (ΔO_2, orange) and bottom pH (ΔpH, black) at a 20 m-deep station off Terrebonne Bay (28.76°N, 90.23°W) in year 4. The change is calculated as future – present.

This change is consistent with the average change in surface waters pH (Table 3) and is a superposition of the biogeochemical and physical effects calculated above.

Total respiration (SOC and water-column respiration combined) did not change in the future simulation and therefore ΔDIC is constant over the normoxic – hypoxic range (Figure 4a); the respiration effect on DIC, i.e., the difference in DIC between oxygen-saturated surface waters and anoxic waters, is $+166$ mmol m^{-3} in both the present and future simulations. However, the respiration effect on pH increases in the future simulation (Figure 4b) because the buffering capacity in the Gulf decreases. The Revelle factor, a measure of buffering capacity where a lower value indicates higher buffering, increases from 9.4 in present-day, oxygen-saturated surface waters in summer to 12.7 in the future. This lowering of the buffering capacity results in a larger effect of respiration on pH in the future, its magnitude increasing from 0.34 in the present simulation to 0.46 in the future (Figure 4b). This result indicates that from the new pH baseline in the northern Gulf waters and independently of the stratification effect, respiration under future conditions will lead to up to 33% more eutrophication-induced acidification than in present conditions.

4. Discussion

Our projection suggests that the northern Gulf of Mexico shelf waters will experience substantial changes by the end of the century. Hypoxia will be more intense and pH will drop significantly (Figure 1). The underlying mechanisms and their sources of variability are discussed below.

4.1. Future Changes in Hypoxic Conditions

Warming of surface waters in the future simulation, in combination with increased freshwater discharge, promotes the development/strengthening of stratification on the shelf. Stratification is a prerequisite for the development of hypoxic conditions in the northern Gulf (Fennel et al., 2013; Wiseman et al., 1997). When shelf waters are stratified, the change in PEA between present and future is correlated with the change in bottom water O_2 and with an increase in hypoxic area, indicating that the strengthening of stratification resulting from climate change will promote the expansion of hypoxia in the future. This result is consistent with the other studies that suggest climate change will induce a general deoxygenation of subsurface waters (Matear & Hirst, 2003), on the order of 1–7% of the global ocean O_2 inventory (Keeling et al., 2010), and in particular in the coastal zone (Conley et al., 2009; Meire et al., 2013). Our results are also

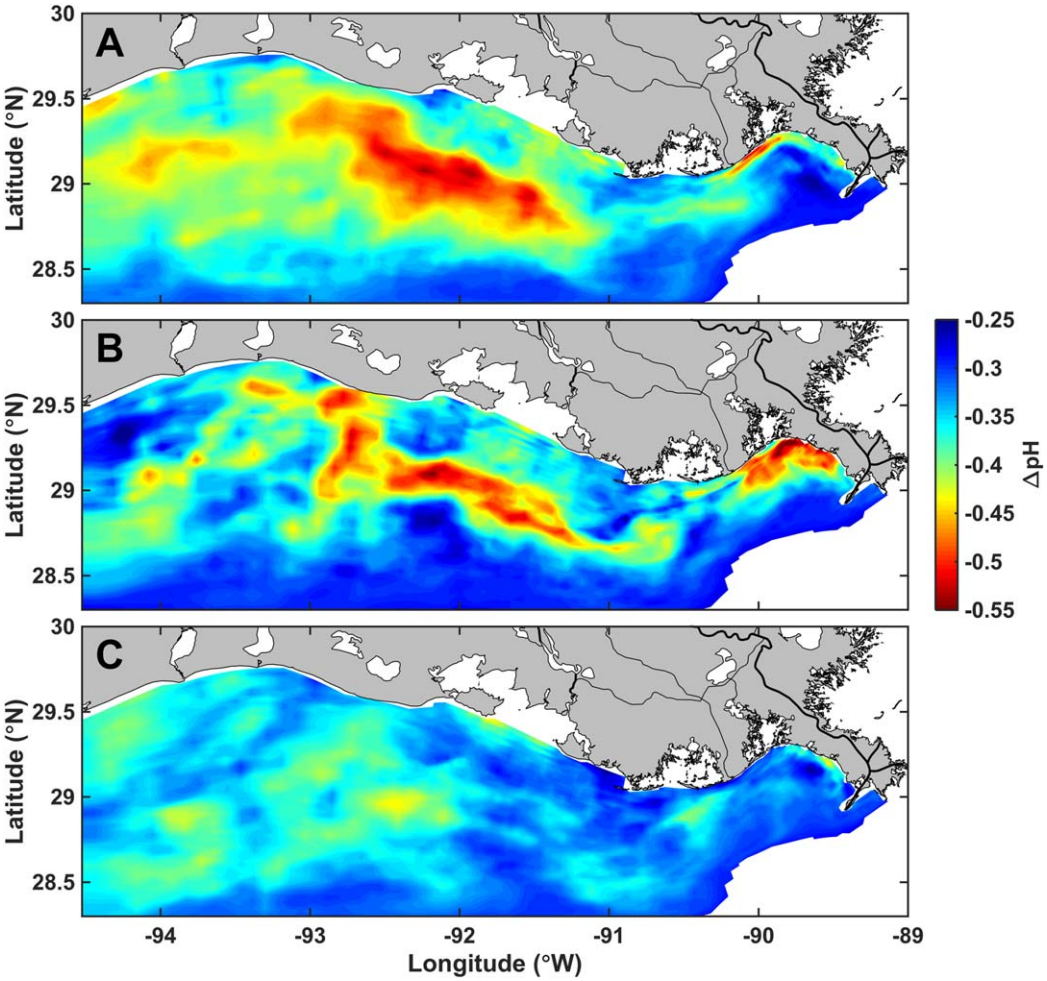

Figure 10. Change in bottom water pH in summer (ΔpH) during the (a) upwelling year, (b) downwelling year, and (c) strong wind year. ΔpH is calculated as future – present.

consistent with previous investigations for the northern Gulf (Justić et al., 1996; Lehrter et al., 2017). In addition to an expansion of the hypoxic area, our results reveal that hypoxic waters will also be more oxygen depleted and larger areas of the shelf will be exposed to hypoxic events for longer. Using different metrics but with similar assumptions about climate change, Lehrter et al. (2017) found that hypoxia will last longer and a larger part of the shelf will be exposed to more than 60 days of hypoxia per year (+8%).

By reviewing O_2 sources and sinks in the present and future simulations, we were able to quantify the contributions of various contributing factors to the oxygen loss of bottom waters. Physical drivers include surface O_2 saturation, stratification, bottom boundary layer thickness, supply from the open ocean, whereas biological sources and sinks are primary production, water-column respiration, nitrification and sediment O_2 consumption. In the northern Gulf, hypoxia mainly occurs near the bottom within the bottom boundary layer and therefore the thickness of the bottom boundary layer influences bottom O_2 and hypoxia (Fennel et al., 2013, 2016). Since changes in stratification and bottom boundary layer thickness (e.g., Figure 8) are closely related, we did not attempt to distinguish their individual contributions; however, the variations in bottom boundary layer thickness are relatively small and stratification is probably the dominant contributor. Overall, changes in stratification and bottom boundary layer thickness contribute 26–40% of the total change in bottom water oxygen, whereas the temperature effect on solubility is the dominant factor (60–74%). This direct effect of increased surface temperatures, which was not diagnosed in previous studies of the northern Gulf, will therefore be a key driver of oxygen loss in this region. As a comparison, in their future projection of the central North Sea, Meire et al. (2013) found that stratification contributed 58% of the change in summer bottom O_2, whereas the temperature effect on O_2 solubility contributed only 27%.

Meire et al. (2013) used bottom O_2 solubility, whereas we used surface O_2 solubility, assuming that surface waters are the O_2 source to subsurface and bottom waters. This distinction may result in a significant difference in our estimates. The remaining difference may be attributed to warmer temperatures in Gulf of Mexico and a larger warming under the RCP8.5 scenario.

Biological oxygen sources and sinks did not have a significant effect on the projected oxygen loss. Perhaps surprising, considering the positive effect of temperature on metabolic processes, this result is consistent with our assumptions. Given the large uncertainty regarding future changes in freshwater discharge and nutrient loads from the Mississippi-Atchafalaya Basin (Sperna Weiland et al., 2012; Tao et al., 2014), we assumed constant nutrient load in the future simulation. We also assumed that SOC is ultimately limited by organic matter supply and thus will not change in the future despite warmer bottom waters. These conservative assumptions limit the influence of biological processes. Assuming a 10% increase in future nutrient load, did not find a significant biological response (in terms of chlorophyll concentration and phytoplankton growth rates) in the study of Lehrter et al. (2017), which also indicates a limited biological contribution to future oxygen changes in their simulation. An additional increase in nutrient load would enhance eutrophication and further deplete bottom oxygen, perhaps making the biological contribution to oxygen loss more important.

4.2. Acidification of the Northern Gulf

Despite their dominant effect on oxygen drawdown, physical changes had only a small effect on the simulated changes in pH, i.e., a contribution $<10\%$ of the total change, with stratification contributing about 6.5% of total ΔpH. The remaining change in pH was mainly due to atmospheric and boundary forcing. These opposite contributions reveal a fundamental difference in the drivers of oxygen loss versus pH changes under future climate forcing. Remote biogeochemical forcing, i.e., high pCO_2 in the atmosphere and carbon-rich offshore waters, will dominate future acidification of the northern Gulf shelf waters and ultimately overwhelm the present eutrophication-induced acidification (e.g., Cai et al., 2011; Laurent et al., 2017). For comparison, the climate-induced acidification of surface and subsurface normoxic waters was $\Delta pH = -0.30$, which is very close to the change in offshore surface pH in the future simulation ($\Delta pH = -0.29$, i.e., from the change in DIC and alkalinity boundary conditions) and to the average change in global surface pH ($\Delta pH = -0.33$) predicted by earth system models (Bopp et al., 2013).

Nevertheless, eutrophication-induced acidification of the northern Gulf remains important in the future and adds to the climate-induced signal (Figure 1). The changes in stratification and pH are correlated, showing an expansion of eutrophication-induced acidification due to physical changes only. Regarding biological processes, we did not expect an intensification of the eutrophication effect on pH because of the assumed constant nutrient loads. The constant relationship between DIC and O_2 (minus the climate effect on DIC) and the lack of a respiration effect on ΔO_2 was a good indication of the constant respiration effect on DIC in the present and future simulations. However, in the future simulation respiration occurs in an acidified ocean with lower buffering capacity; for a same respiration rate, a larger ΔpH occurs in the future simulation. The slope of the O_2 versus pH relationship (Figure 4b) is 1.712×10^{-3} (mol O_2)$^{-1}$ in the present and 2.391×10^{-3} (mol O_2)$^{-1}$ in the future simulation, which represents a 40% increase in the rate of acidification per unit O_2 consumed. This reduced buffering effect on respiration constitutes a strengthening of the eutrophication-induced acidification under future climate and confirms the observations-based projection of Cai et al. (2011). Carbonate saturation was significantly reduced in the future simulation but remained saturated in normoxic waters. Therefore climate-induced ocean acidification alone will not result in undersaturated waters in the northern Gulf. However, aragonite saturation was approaching, and in some cases dropped below, the undersaturation limit in hypoxic waters.

These findings show that despite the overwhelming effect of ocean acidification, eutrophication-induced acidification of bottom waters will remain an important issue in the future because of its additive effect on the climate-induced signal. Locally, it can push the system toward aragonite undersaturation and hypercapnia (i.e., $pCO_2 > 1{,}000$ μatm) which are detrimental to marine organisms (Clements & Hunt, 2015; Flynn et al., 2015; Jutfelt et al., 2013; Mostofa et al., 2016; Nilsson et al., 2012).

4.3. Climate and Interannual Variability

Interannual variability in river discharge and wind forcing is known to be important for hypoxia generation in the northern Gulf, where alongshore and/or freshwater discharge have been correlated with hypoxia

(Feng et al., 2012, 2014; Forrest et al., 2011) and DIC (Huang et al., 2015a). The largest response to future climate occurs in the year with high discharge and upwelling-favorable winds. In contrast, the response is limited in the year with strong winds (except for the climate-induced acidification). Physical forcing promotes enhanced stratification amplifying the effect of climate change on eutrophication-induced oxygen loss and acidification. The wind distribution may vary with climate change (e.g., Bakun et al., 2010, 2015), but there is high uncertainty (Herrera-Estrada & Sheffield, 2017; Wuebbles et al., 2014) and no clear picture for the northern Gulf as of yet (Kulkarni & Huang, 2014; Lehrter et al., 2017). Mixing events may also vary, with fewer but stronger hurricanes projected for the Gulf of Mexico (Bruyère et al., 2017). Future freshwater discharge is relatively uncertain for the northern Gulf as it depends on climate as well as land use changes (Sperna Weiland et al., 2012; Tao et al., 2014). However, increases in weather extremes such as drought and heavy precipitation are a likely effect of climate change (Coumou & Rahmstorf, 2012) and could amplify nutrient load and eutrophication (Lee et al., 2016, Sinha et al., 2017). Our multiannual projection over a typical range of present-day physical conditions does not account for changes in weather extremes but provides a framework to assess the effects of interannual variability and therefore better anticipate the effects of climate change in the northern Gulf.

4.4. Ecological Implications

Compared to other regions, the northern Gulf is less prone to ocean acidification due to its higher buffering capacity. However, marine organisms in the northern Gulf are predicted to have a lower tolerance to small changes in hypercapnic and acidification stress (Feely et al., 2018). Aragonite undersaturation and hypercapnia have mostly negative effects on sensitive species (Gobler & Baumann, 2016; Kroeker et al., 2010), whereas hypoxia results in growth and reproductive impairment (Miller Neilan & Rose, 2014; Thomas & Rahman, 2012). A more frequent exposure to hypoxia, in conjunction with lower aragonite saturation and hypercapnia will likely have a significant impact on a number of calcifying and noncalcifying species and therefore on the ecology of the northern Gulf. These climate-induced changes will be complex and exacerbated by the regional decrease in the metabolic index (i.e., the ratio of O_2 supply to metabolic rate) resulting from the general decline in O_2 (Deutsch et al., 2015).

4.5. Remaining Uncertainties

Several scenarios of anthropogenic CO_2 emissions are used to estimate earth system responses to climate change. We used RCP8.5, which assumes a "business as usual" high CO_2 emissions scenario. More conservative CO_2 emissions scenarios, such as RCP2.6 or RCP4.5, would have smaller effects on the northern Gulf oxygen and pH.

Sea level rise will be incidental to surface warming but is not typically included in future regional projections. Change in sea level may modify significantly the coastline and the location of freshwater discharge, which may further influence eutrophication-induced hypoxia and acidification.

5. Conclusions

Climate change will exacerbate hypoxia and eutrophication-induced acidification in the northern Gulf of Mexico. Climate-driven acidification will ultimately overwhelm the present eutrophication-induced acidification, but eutrophication will remain an important issue that adds to the climate signal. Our model and simulation results provide a deductive framework for understanding the mechanisms that will control oxygen and carbon biogeochemistry in the northern Gulf of Mexico in the future despite the large inherent uncertainties. Current hypoxia mitigation strategies will need to be adapted to take into account climate change effects.

Acknowledgments
Model outputs used in the figures are available in the supporting information. All other data are properly cited and referred to in the reference list. This work was supported by NOAA's Coastal and Ocean Modeling Testbed (COMT) and NOAA CSCOR grants NA06N0S4780198 and NA09N0S4780208. NGOMEX publication number 229.

References

Altieri, A. H., & Gedan, K. B. (2014). Climate change and dead zones. *Global Change Biology*, *21*, 1395–1406. https://doi.org/10.1111/gcb.12754

Aulenbach, B., Buxton, H., Battaglin, W., & Coupe, R. (2007). *Streamflow and nutrient fluxes of the Mississippi-Atchafalaya River basin and subbasins for the period of record through 2005* (Open File Rep. 2007-1080). Reston, VA: U.S. Geological Survey.

Bakun, A., Black, B. A., Bograd, S. J., García-Reyes, M., Miller, A. J., Rykaczewski, R. R., et al. (2015). Anticipated effects of climate change on coastal upwelling ecosystems. *Current Climate Change Reports*, *1*, 85–93. https://doi.org/10.1007/s40641-015-0008-4

Bakun, A., Field, D., Redondo-Rodriguez, A., & Weeks, S. (2010). Greenhouse gas, upwelling-favorable winds, and the future of coastal ocean upwelling ecosystems. *Global Change Biology*, *16*(4), 1213–1228. https://doi.org/10.1111/j.1365-2486.2009.02094.x

Bopp, L., Resplandy, L., Orr, J. C., Doney, S. C., Dunne, J. P., Gehlen, M., et al. (2013). Multiple stressors of ocean ecosystems in the 21st century: Projections with CMIP5 models. *Biogeosciences*, *10*(10), 6225–6245. https://doi.org/10.5194/bg-10-6225-2013

Breitburg, D., Salisbury, J., Bernhard, J. M., Cai, W.-J., Dupont, S., Doney, S. C., et al. (2015). And on top of all that. . . Coping with ocean acidification in the midst of many stressors. *Oceanography*, *25*(2), 48–61. https://doi.org/10.5670/oceanog.2015.31

Bruyère, C. L., Rasmussen, R., Gutmann, E., Done, J., Tye, M., Jaye, A., et al. (2017). *Impact of climate change on Gulf of Mexico hurricanes* (NCAR Tech. Note NCAR/TN-535+STR, 165 pp.). https://doi.org/10.5065/D6RN36J3

Cai, W.-J., Hu, X., Huang, W.-J., Murrell, M. C., Lehrter, J. C., Lohrenz, S. E., et al. (2011). Acidification of subsurface coastal waters enhanced by eutrophication. *Nature Geoscience*, *4*(11), 766–770. https://doi.org/10.1038/ngeo1297

Cheng, L., Trenberth, K. E., Fasullo, J., Boyer, T., Abraham, J., & Zhu, J. (2017). Improved estimates of ocean heat content from 1960 to 2015. *Science Advances*, *3*(3), e1601545. https://doi.org/10.1126/sciadv.1601545

Clements, J., & Hunt, H. (2015). Marine animal behaviour in a high CO_2 ocean. *Marine Ecology Progress Series*, *536*, 259–279. https://doi.org/10.3354/meps11426

Conley, D. J., Carstensen, J., Vaquer-Sunyer, R., & Duarte, C. M. (2009). Ecosystem thresholds with hypoxia. *Hydrobiologia*, *629*(1), 21–29. https://doi.org/10.1007/s10750-009-9764-2

Coumou, D., & Rahmstorf, S. (2012). A decade of weather extremes. *Nature Climate Change*, *2*(7), 491–496. https://doi.org/10.1038/nclimate1452

Da Silva, A., Young, C., & Levitus, S. (1994a). *Atlas of surface marine data 1994, Vol. 3. Anomalies of heat and momentum fluxes* (NOAA Atlas NESDIS 8). Washington, DC: U.S. Dept. Commer.

Da Silva, A., Young, C., & Levitus, S. (1994b). Atlas of surface marine data 1994, *Vol. 4. Anomalies of heat and momentum fluxes* (NOAA Atlas NESDIS 8). Washington, DC: U.S. Dept. Commer.

Deutsch, C., Ferrel, A., Seibel, B., Portner, H.-O., & Huey, R. B. (2015). Climate change tightens a metabolic constraint on marine habitats. *Science*, *348*(6239), 1132–1135. https://doi.org/10.1126/science.aaa1605

Diaz, R. J., & Rosenberg, R. (2008). Spreading dead zones and consequences for marine ecosystems. *Science*, *321*(5891), 926–929. https://doi.org/10.1126/science.1156401

Feely, R., Doney, S., & Cooley, S. (2009). Ocean acidification: Present conditions and future changes in a high-CO_2 world. *Oceanography*, *22*(4), 36–47. https://doi.org/10.5670/oceanog.2009.95

Feely, R., Okazaki, R., Cai, W.-J., Bednaršek, N., Alin, S., Byrne, R., et al. (2018). The combined effects of acidification and hypoxia on pH and aragonite saturation in the coastal waters of the California current ecosystem and the northern Gulf of Mexico. *Continental Shelf Research*, *152*, 50–60. https://doi.org/10.1016/j.csr.2017.11.002

Feng, Y., DiMarco, S. F., & Jackson, G. A. (2012). Relative role of wind forcing and riverine nutrient input on the extent of hypoxia in the northern Gulf of Mexico. *Geophysical Research Letters*, *39*, L09601. https://doi.org/10.1029/2012GL051192

Feng, Y., Fennel, K., Jackson, G. A., DiMarco, S. F., & Hetland, R. D. (2014). A model study of the response of hypoxia to upwelling-favorable wind on the northern Gulf of Mexico shelf. *Journal of Marine Systems*, *131*, 63–73. https://doi.org/10.1016/j.jmarsys.2013.11.009

Fennel, K., Hetland, R., Feng, Y., & DiMarco, S. (2011). A coupled physical-biological model of the northern Gulf of Mexico shelf: Model description, validation and analysis of phytoplankton variability. *Biogeosciences*, *8*(7), 1881–1899. https://doi.org/10.5194/bg-8-1881-2011

Fennel, K., Hu, J., Laurent, A., Marta-Almeida, M., & Hetland, R. (2013). Sensitivity of hypoxia predictions for the northern Gulf of Mexico to sediment oxygen consumption and model nesting. *Journal of Geophysical Research: Oceans*, *118*, 990–1002. https://doi.org/10.1002/jgrc.20077

Fennel, K., Laurent, A., Hetland, R., Justić, D., Ko, D. S., Lehrter, J., et al. (2016). Effects of model physics on hypoxia simulations for the northern Gulf of Mexico: A model intercomparison. *Journal of Geophysical Research: Oceans*, *121*, 5731–5750. https://doi.org/10.1002/2015JC011577

Fennel, K., Wilkin, J., Levin, J., Moisan, J., O'Reilly, J., & Haidvogel, D. (2006). Nitrogen cycling in the Middle Atlantic Bight: Results from a three-dimensional model and implications for the North Atlantic nitrogen budget. *Global Biogeochemical Cycles*, *20*, GB3007. https://doi.org/10.1029/2005GB002456

Fennel, K., Wilkin, J., Previdi, M., & Najjar, R. (2008). Denitrification effects on air-sea CO_2 flux in the coastal ocean: Simulations for the northwest North Atlantic. *Geophysical Research Letters*, *35*, L24608. https://doi.org/10.1029/2008GL036147

Flynn, K. J., Clark, D. R., Mitra, A., Fabian, H., Hansen, P. J., Glibert, P. M., et al. (2015). Ocean acidification with (de)eutrophication will alter future phytoplankton growth and succession. *Proceedings. Biological Sciences*, *282*(1804), 20142604. https://doi.org/10.1098/rspb.2014.2604

Forrest, D. R., Hetland, R. D., & DiMarco, S. F. (2011). Multivariable statistical regression models of the areal extent of hypoxia over the Texas–Louisiana continental shelf. *Environmental Research Letters*, *6*(4), 45002. https://doi.org/10.1088/1748-9326/6/4/045002

Giorgetta, M. A., Jungclaus, J., Reick, C. H., Legutke, S., Bader, J., Böttinger, M., et al. (2013). Climate and carbon cycle changes from 1850 to 2100 in MPI-ESM simulations for the Coupled Model Intercomparison Project phase 5. *Journal of Advances in Modeling Earth Systems*, *5*, 572–597. https://doi.org/10.1002/jame.20038

Gobler, C. J., & Baumann, H. (2016). Hypoxia and acidification in ocean ecosystems: Coupled dynamics and effects on marine life. *Biology Letters*, *12*(5), 20150976., https://doi.org/10.1098/rsbl.2015.0976

Haidvogel, D. B., Arango, H., Budgell, W. P., Cornuelle, B. D., Curchitser, E., Di Lorenzo, E., et al. (2008). Ocean forecasting in terrain-following coordinates: Formulation and skill assessment of the Regional Ocean Modeling System. *Journal of Computational Physics*, *227*(7), 3595–3624. https://doi.org/10.1016/j.jcp.2007.06.016

Herrera-Estrada, J. E., & Sheffield, J. (2017). Uncertainties in future projections of summer droughts and heat waves over the Contiguous United States. *Journal of Climate*, *30*(16), 6225–6246. https://doi.org/10.1175/JCLI-D-16-0491.1

Hetland, R. D., & DiMarco, S. F. (2008). How does the character of oxygen demand control the structure of hypoxia on the Texas–Louisiana continental shelf? *Journal of Marine Systems*, *70*(1–2), 49–62. https://doi.org/10.1016/j.jmarsys.2007.03.002

Hetland, R. D., & DiMarco, S. F. (2012). Skill assessment of a hydrodynamic model of circulation over the Texas–Louisiana continental shelf. *Ocean Modelling*, *43–44*, 64–76. https://doi.org/10.1016/j.ocemod.2011.11.009

Huang, W.-J., Cai, W.-J., Wang, Y., Hu, X., Chen, B., Lohrenz, S. E., et al. (2015a). The response of inorganic carbon distributions and dynamics to upwelling-favorable winds on the northern Gulf of Mexico during summer. *Continental Shelf Research*, *111*, 211–222. https://doi.org/10.1016/j.csr.2015.08.020

Huang, W.-J., Cai, W.-J., Wang, Y., Lohrenz, S. E., & Murrell, M. C. (2015b). The carbon dioxide system on the Mississippi River-dominated continental shelf in the northern Gulf of Mexico: 1. Distribution and air-sea CO_2 flux. *Journal of Geophysical Research: Oceans*, *120*, 1429–1445. https://doi.org/10.1002/2014JC010498

Ilyina, T., Six, K. D., Segschneider, J., Maier-Reimer, E., Li, H., & Núñez-Riboni, I. (2013). Global ocean biogeochemistry model HAMOCC: Model architecture and performance as component of the MPI-Earth system model in different CMIP5 experimental realizations. *Journal of Advances in Modeling Earth Systems*, *5*, 287–315. https://doi.org/10.1029/2012MS000178

Justić, D., Rabalais, N., & Turner, R. E. (1996). Effects of climate change on hypoxia in coastal waters: A doubled CO_2 scenario for the northern Gulf of Mexico. *Limnology and Oceanography*, *41*(5), 992–1003. https://doi.org/10.4319/lo.1996.41.5.0992

Jutfelt, F., Bresolin de Souza, K., Vuylsteke, A., & Sturve, J. (2013). Behavioural disturbances in a temperate fish exposed to sustained high-CO_2 levels, *PLoS ONE*, *8*(6), e65825. https://doi.org/10.1371/journal.pone.0065825

Keeling, R. E., Körtzinger, A., & Gruber, N. (2010). Ocean deoxygenation in a warming world. *Annual Review of Marine Science*, *2*, 199–229. https://doi.org/10.1146/annurev.marine.010908.163855

Ko, D. S., Preller, R. H., & Martin, J. P. (2003). An experimental real-time Intra-Americas Sea Ocean Nowcast/Forecast System for coastal prediction. In *AMS 5th Conference on Coastal Atmospheric and Oceanic Prediction and Processes* (pp. 97–100). Boston, MA: American Mathematical Society.

Ko, D. S., & Wang, D. P. (2014). *Intra-Americas Sea Nowcast/Forecast System ocean reanalysis to support improvement of oil-spill risk analysis in the Gulf of Mexico by multi-model approach* (Rep. BOEM 2014-1003, 55 pp.). Herndon, VA: Department of the Interior, Bureau of Ocean Energy Management. Retrieved from http://www.data.boem.gov/PI/PDFImages/ESPIS/5/5447.pdf

Kroeker, K. J., Kordas, R. L., Crim, R. N., & Singh, G. G. (2010). Meta-analysis reveals negative yet variable effects of ocean acidification on marine organisms. *Ecology Letters*, *13*(11), 1419–1434. https://doi.org/10.1111/j.1461-0248.2010.01518.x

Kulkarni, S., & Huang, H.-P. (2014). Changes in surface wind speed over North America from CMIP5 model projections and implications for wind energy. *Advances in Meteorology*, *2014*, 1–10. https://doi.org/10.1155/2014/292768

Laurent, A., & Fennel, K. (2014). Simulated reduction of hypoxia in the northern Gulf of Mexico due to phosphorus limitation. *Elementa: Science of the Anthropocene*, *2*(1), 22. https://doi.org/10.12952/journal.elementa.000022

Laurent, A., & Fennel, K. (2017). Modeling river-induced phosphorus limitation in the context of coastal hypoxia. In D. Justic, K. Rose, R. Hetland, & K. Fennel (Eds.), *Modeling coastal hypoxia* (pp. 173–214). Cham, Switzerland: Springer. https://doi.org/10.1007/978-3-319-54571-4_7

Laurent, A., Fennel, K., Cai, W.-J., Huang, W.-J., Barbero, L., & Wanninkhof, R. (2017). Eutrophication-induced acidification of coastal waters in the northern Gulf of Mexico: Insights into origin and processes from a coupled physical-biogeochemical model. *Geophysical Research Letters*, *44*, 946–956. https://doi.org/10.1002/2016GL071881

Laurent, A., Fennel, K., Hu, J., & Hetland, R. (2012). Simulating the effects of phosphorus limitation in the Mississippi and Atchafalaya River plumes. *Biogeosciences*, *9*(11), 4707–4723. https://doi.org/10.5194/bg-9-4707-2012

Laurent, A., Fennel, K., Wilson, R., Lehrter, J., & Devereux, R. (2016). Parameterization of biogeochemical sediment–water fluxes using in situ measurements and a diagenetic model. *Biogeosciences*, *13*(1), 77–94. https://doi.org/10.5194/bg-13-77-2016

Lee, M., Shevliakova, E., Malyshev, S., Milly, P. C. D., & Jaffé, P. R. (2016). Climate variability and extremes, interacting with nitrogen storage, amplify eutrophication risk. *Geophysical Research Letters*, *43*, 7520–7528. https://doi.org/10.1002/2016GL069254

Lehrter, J. C., Ko, D. S., Lowe, L. L., & Penta, B. (2017). Predicted effects of climate change on northern Gulf of Mexico hypoxia. In D. Justic, K. Rose, R. Hetland, & K. Fennel (Eds.), *Modeling coastal hypoxia* (pp. 173–214). Cham, Switzerland: Springer. https://doi.org/10.1007/978-3-319-54571-4_8

Levin, L. A., Liu, K.-K., Emeis, K.-C., Breitburg, D. L., Cloern, J., Deutsch, C., et al. (2015). Comparative biogeochemistry–ecosystem–human interactions on dynamic continental margins. *Journal of Marine Systems*, *141*, 3–17. https://doi.org/10.1016/j.jmarsys.2014.04.016

Marta-Almeida, M., Hetland, R. D., & Zhang, X. (2013). Evaluation of model nesting performance on the Texas-Louisiana continental shelf. *Journal of Geophysical Research: Oceans*, *118*, 1–16. https://doi.org/10.1002/jgrc.20163

Matear, R. J., & Hirst, A. C. (2003). Long-term changes in dissolved oxygen concentrations in the ocean caused by protracted global warming. *Global Biogeochemical Cycles*, *17*(4), 1125. https://doi.org/10.1029/2002GB001997

Mattern, J. P., Fennel, K., & Dowd, M. (2013). Sensitivity and uncertainty analysis of model hypoxia estimates for the Texas-Louisiana shelf. *Journal of Geophysical Research: Oceans*, *118*, 1316–1332. https://doi.org/10.1002/jgrc.20130

Meire, L., Soetaert, K. E. R., & Meysman, F. J. R. (2013). Impact of global change on coastal oxygen dynamics and risk of hypoxia. *Biogeosciences*, *10*(4), 2633–2653. https://doi.org/10.5194/bg-10-2633-2013

Melzner, F., Thomsen, J., Koeve, W., Oschlies, A., Gutowska, M. A., Bange, H. W., et al. (2013). Future ocean acidification will be amplified by hypoxia in coastal habitats. *Marine Biology*, *160*(8), 1875–1888. https://doi.org/10.1007/s00227-012-1954-1

Mesinger, F., DiMego, G., Kalnay, E., Mitchell, K., Shafran, P. C., Ebisuzaki, W., et al. (2006). North American regional reanalysis. *Bulletin of the American Meteorological Society*, *87*(3), 343–360. https://doi.org/10.1175/BAMS-87-3-343

Miller Neilan, R., & Rose, K. (2014). Simulating the effects of fluctuating dissolved oxygen on growth, reproduction, and survival of fish and shrimp. *Journal of Theoretical Biology*, *343*, 54–68. https://doi.org/10.1016/j.jtbi.2013.11.004

Mostofa, K. M. G., Liu, C.-Q., Zhai, W. D., Minella, M., Vione, D., Gao, K., et al. (2016). Reviews and syntheses: Ocean acidification and its potential impacts on marine ecosystems. *Biogeosciences*, *13*(6), 1767–1786. https://doi.org/10.5194/bg-13-1767-2016

Nilsson, G. E., Dixson, D. L., Domenici, P., McCormick, M. I., Sørensen, C., Watson, S.-A., et al. (2012). Near-future carbon dioxide levels alter fish behaviour by interfering with neurotransmitter function. *Nature Climate Change*, *2*(3), 201–204. https://doi.org/10.1038/nclimate1352

Rabalais, N. N., Díaz, R. J., Levin, L. A., Turner, R. E., Gilbert, D., & Zhang, J. (2010). Dynamics and distribution of natural and human-caused hypoxia. *Biogeosciences*, *7*(2), 585–619. https://doi.org/10.5194/bg-7-585-2010

Rabalais, N. N., Turner, R. E., Sen Gupta, B. K., Boesch, D. F., Chapman, P., & Murrell, M. C. (2007). Hypoxia in the northern Gulf of Mexico: Does the science support the plan to reduce, mitigate, and control hypoxia? *Estuaries and Coasts*, *30*(5), 753–772. https://doi.org/10.1007/BF02841332

Rabouille, C., Conley, D. J., Dai, M. H., Cai, W.-J., Chen, C. T. A., Lansard, B., et al. (2008). Comparison of hypoxia among four river-dominated ocean margins: The Changjiang (Yangtze), Mississippi, Pearl, and Rhône rivers. *Continental Shelf Research*, *28*(12), 1527–1537. https://doi.org/10.1016/j.csr.2008.01.020

Riahi, K., Rao, S., Krey, V., Cho, C., Chirkov, V., Fischer, G., et al. (2011). RCP 8.5—A scenario of comparatively high greenhouse gas emissions. *Climatic Change*, *109*(1–2), 33–57. https://doi.org/10.1007/s10584-011-0149-y

Sarmiento, J. L., Hughes, T. M. C., Stouffer, R. J., & Manabe, S. (1998). Simulated response of the ocean carbon cycle to anthropogenic climate warming. *Nature*, *393*(6682), 245–249. https://doi.org/10.1038/30455

Sinha, E., Michalak, A. M., & Balaji, V. (2017). Eutrophication will increase during the 21st century as a result of precipitation changes. *Science*, *357*(6349), 405–408. https://doi.org/10.1126/science.aan2409

Sperna Weiland, F. C., van Beek, L. P. H., Kwadijk, J. C. J., & Bierkens, M. F. P. (2012). Global patterns of change in discharge regimes for 2100. *Hydrology and Earth System Sciences*, *16*(4), 1047–1062. https://doi.org/10.5194/hess-16-1047-2012

Tao, B., Tian, H., Ren, W., Yang, J., Yang, Q., He, R., et al. (2014). Increasing Mississippi River discharge throughout the 21st century influenced by changes in climate, land use, and atmospheric CO_2. *Geophysical Research Letters*, *41*, 4978–4986. https://doi.org/10.1002/2014GL060361

Thomas, P., & Rahman, M. S. (2012). Extensive reproductive disruption, ovarian masculinization and aromatase suppression in Atlantic croaker in the northern Gulf of Mexico hypoxic zone. *Proceedings of the Royal Society B: Biological Sciences*, *279*(1726), 28–38. https://doi.org/10.1098/rspb.2011.0529

Wanninkhof, R. (2014). Relationship between wind speed and gas exchange over the ocean revisited. *Limnology and Oceanography Methods*, *12*(6), 351–362. https://doi.org/10.4319/lom.2014.12.351

Wiseman, W. J., Rabalais, N. N., Turner, R. E., Dinnel, S. P., & MacNaughton, A. (1997). Seasonal and interannual variability within the Louisiana coastal current: Stratification and hypoxia. *Journal of Marine Systems*, *12*, 237–248. https://doi.org/10.1016/S0924-7963(96)00100-5

Wuebbles, D., Meehl, G., Hayhoe, K., Karl, T. R., Kunkel, K., Santer, B., et al. (2014). CMIP5 climate model analyses: Climate extremes in the United States. *Bulletin of the American Meteorological Society*, *95*(4), 571–583. https://doi.org/10.1175/BAMS-D-12-00172.1

Yu, L., Fennel, K., & Laurent, A. (2015a). A modeling study of physical controls on hypoxia generation in the northern Gulf of Mexico. *Journal of Geophysical Research: Oceans*, *120*, 5019–5039. https://doi.org/10.1002/2014JC010634

Yu, L., Fennel, K., Laurent, A., Murrell, M. C., & Lehrter, J. C. (2015b). Numerical analysis of the primary processes controlling oxygen dynamics on the Louisiana shelf. *Biogeosciences*, *12*(7), 2063–2076. https://doi.org/10.5194/bg-12-2063-2015